Journal of Chromatography A, 1229 (2012) 113–120

Contents lists available at SciVerse ScienceDirect

Journal of Chromatography A

journal homepage: www.elsevier.com/locate/chroma

Probing multimodal ligand binding regions on ubiquitin using nuclear magnetic resonance, chromatography, and molecular dynamics simulations☆

Melissa A. Holstein[a], Wai Keen Chung[a], Siddharth Parimal[a], Alexander S. Freed[a], Blanca Barquera[b], Scott A. McCallum[b], Steven M. Cramer[a,*]

[a] Rensselaer Polytechnic Institute, Center for Biotechnology and Interdisciplinary Studies, Howard P. Isermann Department of Chemical and Biological Engineering, USA
[b] Rensselaer Polytechnic Institute, Center for Biotechnology and Interdisciplinary Studies, Department of Biology, USA

ARTICLE INFO

Article history:
Received 4 September 2011
Received in revised form
15 November 2011
Accepted 23 December 2011
Available online 9 January 2012

Keywords:
Multimodal chromatography
Nuclear magnetic resonance
Chemical shift perturbation mapping
Site-directed mutagenesis
Molecular dynamics simulations

ABSTRACT

Site-directed mutagenesis, nuclear magnetic resonance (NMR) chemical shift perturbation experiments, and molecular dynamics (MD) simulations are employed in concert with chromatographic experiments to provide insight into protein–ligand interactions in multimodal chromatographic systems. In previous studies, a preferred binding region was identified on the surface of the protein ubiquitin for binding with a multimodal ligand. In this study, site-directed mutagenesis is used to enable direct NMR evaluation of the mutant protein as compared to the wild type. It is found that reversing the charge of a key residue (K6E) in the proposed preferred binding region results in substantial decreases in the magnitude of the ligand-induced NMR chemical shift perturbations relative to those detected for the wild type protein, particularly for residues located within the preferred binding region. These NMR results also indicate a decrease in ligand affinity, consistent with the weaker chromatographic retention observed for the mutant as compared to the wild type on a multimodal cation exchange resin. MD simulation results provide additional insight at a molecular level and demonstrate that many residues located within the preferred binding region exhibit weaker binding interactions due to the mutation. The analysis suggests that multimodal ligand binding consists of initial localization of the ligand by long-ranged electrostatic interactions followed by multiple short-ranged synergistic interactions to attain high affinities of the ligand to specific residues.

1. Introduction

Recent advances in the design of multimodal chromatographic systems have produced unique classes of chromatographic materials capable of providing alternative and improved affinities and selectivities as compared to traditional single-mode chromatographic materials such as ion exchangers [1–10]. Multimodal chromatographic materials have the potential to create more streamlined bioseparation processes, which are crucial for the production of high purity pharmaceuticals and therapeutics.

The selectivity for separations of biomolecules such as peptides [2], oligonucleotides [11], nucleic acids [12,13], and oligomer-like compounds [14] has been significantly improved through the use of multimodal chromatographic materials. Furthermore, multimodal resins have also been shown to enhance product quality, and to improve process efficiency in industrial-scale monoclonal antibody manufacturing processes [15]. Kaleas et al. employed a multimodal cation exchange resin at pilot and manufacturing scales to selectively capture a human growth factor protein from a challenging feedstock with minimal load conditioning. The multimodal purification step produced a low refold pool volume and a high yield while reducing host cell protein content [16].

Ligand-induced chemical shift perturbations are routinely employed for identifying ligand binding sites on protein surfaces using NMR [17]. The high sensitivity of chemical shifts to changes in the local electronic environment makes it possible to detect ligand association at an atomic level and also provides an accurate determination of binding affinity [18–25]. Further, differences in protein–ligand binding behavior among native and mutant proteins are frequently revealed through the detection of altered ligand-induced chemical shift changes [26–28]. Recently, the differences in protein binding behavior on an ion exchange and a multimodal chromatographic resin were examined using a homologous library of cold shock protein B mutants [29]. Moreover, the underlying nature of protein binding in ion exchange and multimodal chromatographic systems was investigated using NMR experiments and coarse-grained ligand docking simulations in concert with chromatographic data for a commercial library of

☆ Presented at the 24th International Symposium on Preparative and Process Chromatography, Boston, MA, USA, 10–13 July 2011.

* Corresponding author. Tel.: +1 518 276 6198; fax: +1 518 276 4030.
E-mail address: crames@rpi.edu (S.M. Cramer).

0021-9673/$ – see front matter © 2012 Elsevier B.V. All rights reserved.
doi:10.1016/j.chroma.2011.12.101

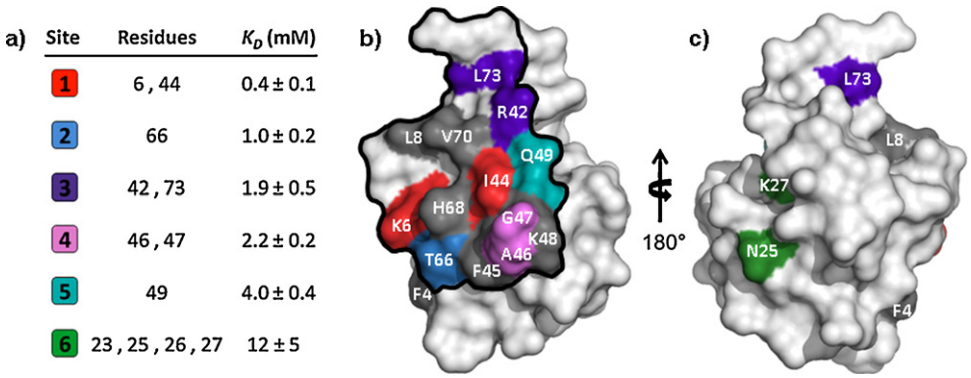

Fig. 1. Multimodal ligand binding sites identified by NMR for human ubiquitin. (a) Color-coded binding sites denoting the associated residues, the average dissociation constants (K_D), and the standard error of the fitted K_D values. (b and c) Front and back surface representations of ubiquitin displaying color-coded ligand binding sites. Residues that displayed multiphasic behavior are depicted in grey. A proposed preferred binding region is outlined in black. (For interpretation of the references to color in this figure legend, the reader is referred to the web version of the article.)
Figure reproduced from Ref. [30].

ubiquitin mutants [30]. In this previous study with ubiquitin, sites of specific protein–multimodal ligand interaction were identified and ranked based on binding affinity. Fig. 1 presents a surface representation of ubiquitin colored according to the experimentally determined binding sites. One high affinity site was identified with an apparent dissociation constant of 0.4 mM (±0.1 mM), along with several surrounding binding sites of intermediate affinity. The clustering of binding sites and geometrical considerations led to the proposition of a preferred binding region on the ubiquitin surface. This region is outlined in black in Fig. 1.

Molecular dynamics simulation has proved to be a powerful tool for characterizing protein–ligand interactions, including the prediction of ligand binding to proteins with unique surface topographies such as cavities [31]. We have recently used molecular dynamics simulations of ubiquitin in aqueous solution containing ligands in free solution to identify binding preferences and to shed light on the 'pseudo-affinity' nature of multimodal interactions [32]. These results suggested that water-mediated electrostatic interactions may be more important for the localization of the multimodal ligand to the binding region with additional stability provided by a combination of local interactions such as hydrophobicity and hydrogen bonding.

Our approach of using NMR experiments in concert with chromatographic data and molecular modeling provides a multi-faceted approach for probing the structural basis of protein adsorption in multimodal chromatographic systems. The current study further examines the role of a proposed key charged residue (Lys 6) within the preferred binding region on ubiquitin using site-directed mutagenesis to enable direct NMR evaluation of the mutant protein as compared to the wild type. This residue was not only located within the proposed preferred binding region, but also it is one of the two residues that comprised the high affinity binding site and was therefore predicted to play an important role in the protein–ligand binding interactions. In addition, molecular dynamics simulations are also conducted with the wild type and mutant proteins to provide further insight into the nature of binding in this multimodal system.

2. Materials and methods

2.1. Materials

Capto MMC media was obtained from GE Healthcare (Uppsala, Sweden) and packed into a Pharmacia Biotech glass column (5 mm × 50 mm). Sodium chloride, acetic acid, sodium acetate, deuterium oxide (D_2O), 3-(trimethylsilyl)propionic acid-d_4 sodium salt (TMSP), NMR tubes, and N-benzoyl-DL-methionine were purchased from Sigma–Aldrich (St. Louis, MO). A QuikChange Lightning Site-Directed Mutagenesis Kit was obtained from Stratagene (Agilent Technologies, Santa Clara, CA). Primers were ordered from Invitrogen (Carlsbad, CA). A Wizard Plus SV Miniprep kit was purchased from Promega (Madison, WI).

2.2. Equipment

Analytical linear gradient experiments were performed using a Waters HPLC system consisting of a 600 multi-solvent delivery system, a 717 WISP autoinjector, and a 996 photodiode array detector controlled by a Millennium chromatography software manager. NMR spectra were obtained at 25 °C using a Bruker Avance II 800-MHz spectrometer equipped with a $^1H/^{13}C/^{15}N$ cryoprobe with *z*-axis gradients.

2.3. Methods

2.3.1. Linear gradient chromatography

Linear gradient chromatography experiments were carried out at room temperature on a multimodal cation exchange (Capto MMC) resin. For these experiments, the linear salt gradient transitioned from buffer A (20 mM sodium acetate, pH 5) to buffer B (20 mM sodium acetate, 1.5 M sodium chloride, pH 5) over 60 column volumes. A flowrate of 1 mL/min and a column volume of 1 mL were used in all experiments. The column effluent was monitored using UV absorbance at 280 nm.

2.3.2. PCR-based site-directed mutagenesis

A ubiquitin mutant (K6E) was generated using the wild type ubiquitin gene (cloned into the pET 15b vector) as a template. The following primers were used: forward (5′-GATCCATGCAGATCTTCGTCGAAACGTTAACCGGTAAAACCAT-3′), reverse (5′-ATGGTTTTACCGGTTAACGTTTCGACGAAGATCTGCATGGATC-3′). Site-directed mutagenesis was carried out using the QuikChange Lightning Site-Directed Mutagenesis Kit (Stratagene).

The final mutagenesis product was used to transform *Escherichia coli* XL10-Gold ultracompetent cells, which were plated onto LB (Luria Bertani, Miller) agar plates containing ampicillin (100 μg/mL) and incubated at 37 °C. Five clones were isolated and grown in liquid LB medium containing ampicillin (100 μg/mL). Plasmid was isolated using a Promega Wizard Plus SV Miniprep kit. The plasmid DNA was sequenced to confirm the introduction of the desired mutation. *E. coli* BL21(DE3) cells were then transformed with the mutated plasmid.

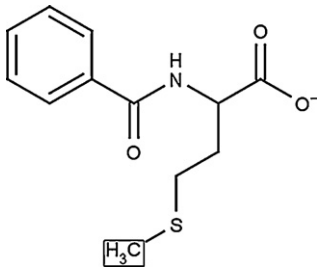

Fig. 2. Chemical structure of a representative multimodal cation exchange chromatographic ligand, N-benzoyl-DL-methionine (note: the point where the ligand would be immobilized to an agarose base matrix is indicated by a box).

2.3.3. Protein expression and purification

Uniformly $^{13}C/^{15}N$-enriched wild type recombinant ubiquitin was expressed using the BL21(DE3) strain of *E. coli* and purified as described by Chung et al. [30]. The expression and purification protocols for the mutant ubiquitin K6E were similar to those previously described for the wild type protein [30]. However, two purification steps were adjusted due to a difference in the protein isoelectric point (pI) of the wild type and mutant proteins. In the case of the mutant variant, the pH was lowered to 4 during the acid precipitation step and the cation exchange chromatographic experiments. All other expression and purification steps remained unaltered. The final protein concentration was determined by spectrophotometric analysis at 280 nm with a molar extinction coefficient of 1490 M^{-1} cm^{-1} [33].

2.3.4. NMR chemical shift perturbation mapping

NMR data were acquired and processed using Bruker TopSpin 2.1 software and analyzed using the software package Sparky [34]. Assignments of amide resonances were confirmed by matching published chemical shift values (BMRB accession number 6457) with backbone correlation patterns detected in spectra of unbound protein. $^{1}H–^{15}N$ HSQC spectra were acquired where each sample had an initial volume of 400 μL and contained 0.1 mM isotopically enriched ubiquitin in NMR buffer (10 mM sodium acetate, pH 5.0, 0.02% sodium azide, 1 μM TMSP as an internal standard, and 5% D_2O) with varying concentrations of a multimodal ligand (N-benzoyl-DL-methionine). This model soluble ligand is structurally equivalent to the functional moieties of the immobilized resin material with the exception of a modification at the resin linkage point indicated by a box (Fig. 2). Due to the limited solubility of the ligand, the maximum ligand concentration was limited to 3.2 mM. The maximum change in weighted average chemical shift ($\Delta\delta_{NH} = ((\Delta\delta_H)^2 + (0.2\cdot\Delta\delta_N)^2)^{1/2}$) was calculated for each amide group detected free of spectral overlap in the NMR experiment that was detected to undergo ligand-induced changes in chemical shift [35,36]. Protein visualization was carried out with PyMOL [37].

2.3.5. Molecular dynamics simulations

All-atom MD simulations were performed with human ubiquitin and mutant K6E separately to analyze their interactions with the multimodal ligand. The initial structural model for these studies was obtained from a deposited crystal structure of human ubiquitin in the RCSB Protein Data Bank (PDB ID: 1D3Z). The protonation states of ionizable residues corresponded to a pH of 5. At this pH, lysines, arginines, and histidines were positively charged, whereas glutamic acids and aspartic acids were negatively charged, resulting in an overall charge of +1e for wild type ubiquitin and −1e for the mutant K6E. Each simulation was confined to a 7 nm × 7 nm × 7 nm box containing one protein molecule, six multimodal ligand molecules, an appropriate number of counter-ions added to make the system electrically neutral, and a large number of water molecules. The six ligand molecules in a simulation box were placed randomly around the protein molecule and sufficiently far away (>2 nm) to minimize the effect of starting orientations. This procedure was repeated six times to obtain six different starting configurations of the system for MD simulations.

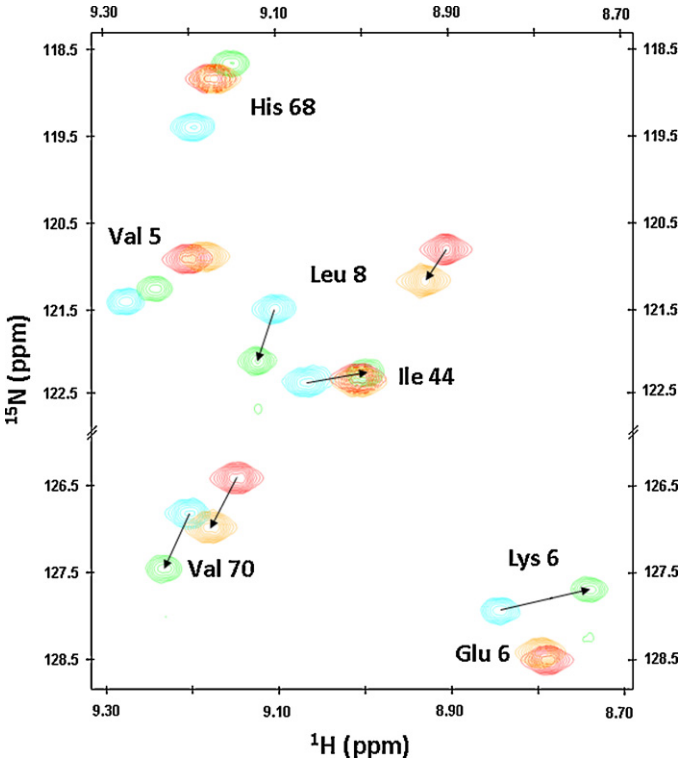

Fig. 3. Selected $^{1}H–^{15}N$ HSQC spectra for the wild type and mutant proteins. Spectra obtained for wild type ubiquitin in the absence (blue) and presence (green) of the multimodal ligand are shown for selected residues. Spectra are also shown for the mutant protein in the absence (red) and presence (orange) of the multimodal ligand. (For interpretation of the references to color in this figure legend, the reader is referred to the web version of the article.)

The force field used for the protein was AMBER 94 [38]. For obtaining an initial structural model of mutant K6E, the MOE [39] software package was used to introduce the mutation at the sixth residue followed by energy-minimization of the structure. For the ligands, parameters were taken from previous work by our group [32]. The SPC/E [40] model was used to describe water explicitly.

Each system was initially energy-minimized using the steepest descent algorithm before performing MD simulations in the isothermal–isobaric (N,P,T) ensemble using the GROMACS 3.3.3 molecular dynamics package [41,42]. Temperature (300 K) and pressure (1 bar) were maintained using the Nose–Hoover thermostat [43,44] and Parrinello–Rahman barostat [45], respectively. Periodic boundary conditions were applied in all three directions. A cutoff of 1 nm was used for all LJ interactions. The Particle Mesh Ewald (PME) method [46] was used to calculate electrostatic interactions. A time step of 2 fs was used for all MD simulations. Each of the six configurations was simulated for 40 ns, providing data for a total of 240 ns. The software packages VMD [47] and PyMOL [37] were used for visualization and simulation setup.

3. Results and discussion

As described in the introduction, previous work in our lab has provided evidence that the protein ubiquitin has a preferred binding face for interacting with the Capto MMC multimodal ligand in both solution and solid phase systems. The current study further probes the role of a proposed key residue of the high affinity binding

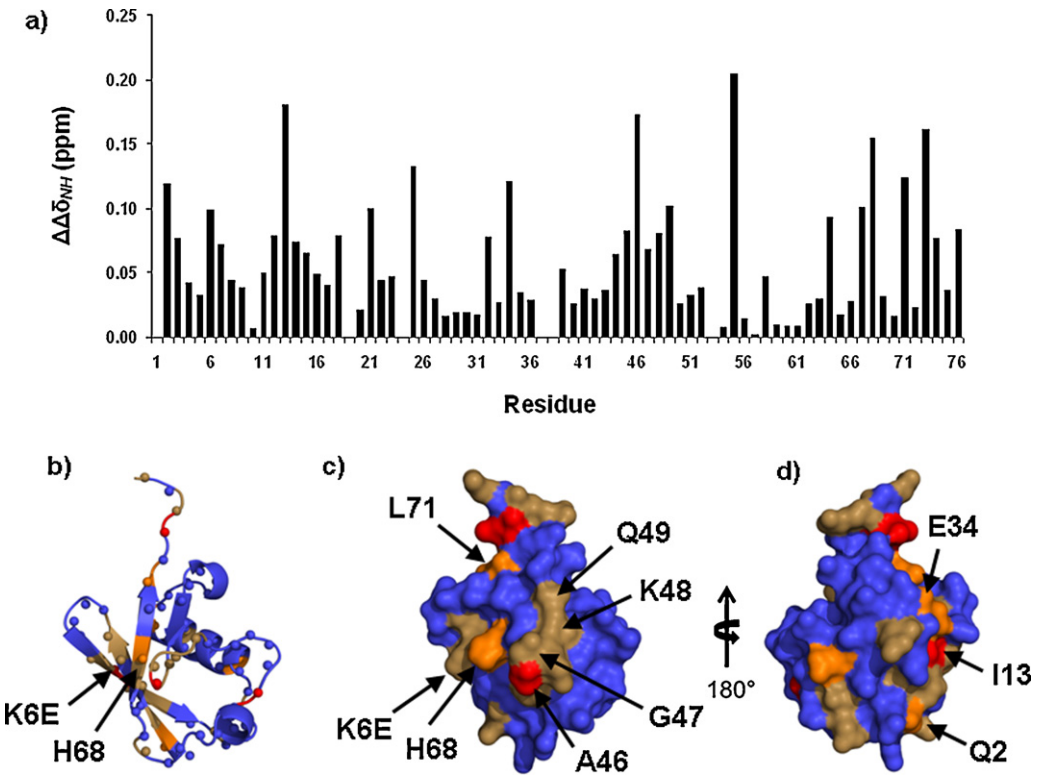

Fig. 4. Difference between the maximum ligand-induced changes in the weighted average chemical shift ($\Delta\Delta\delta_{NH}$) between wild type ubiquitin and mutant K6E for the binding of a multimodal cation exchange ligand. (a) Plot of $\Delta\Delta\delta_{NH}$ as a function of residue number; (b) Ribbon representation of ubiquitin with the position of amide nitrogen reporter atoms shown as small spheres and colored according to $\Delta\Delta\delta_{NH}$; (c and d) Front and back surface representations of ubiquitin, respectively. A uniform red–orange–brown–blue color scale is employed denoting large (red, $\Delta\Delta\delta_{NH} > 0.15$), moderate (orange, $0.10 < \Delta\Delta\delta_{NH} < 0.15$), small (brown, $0.07 < \Delta\Delta\delta_{NH} < 0.10$), and minimal (blue, $\Delta\Delta\delta_{NH} < 0.07$) differences between the weighted average chemical shift perturbations for the wild type and mutant proteins. (For interpretation of the references to color in this figure legend, the reader is referred to the web version of the article.)

site located within the preferred binding region using site-directed mutagenesis in conjunction with chromatography, NMR chemical shift perturbation mapping, and molecular dynamics simulations.

3.1. Chromatographic retention behavior

The wild type ubiquitin contains a lysine residue at position 6, which was previously determined to be located in the proposed preferred binding region [30]. The ubiquitin mutant K6E was recombinantly expressed and purified as described in Section 2. Chromatography was then carried out to compare the retention behavior of this mutant variant toward the wild type on the Capto MMC multimodal resin. The results indicate that mutant K6E exhibited much weaker retention, with a gradient elution salt concentration of 0.47 M NaCl as compared to 1.37 M for the wild type. While one would expect that reversing the charge on residue 6 might decrease binding due to reduced electrostatic interactions and possible electrostatic repulsions in the local region, this should only be important if that region of the protein surface is directly involved in resin binding. These chromatographic results clearly demonstrate that this site is indeed playing an important role in the interaction of ubiquitin with the multimodal resin. This is consistent with previous results where mutations to lysine residues located within the preferred binding region led to major changes in protein retention while mutations to lysine residues located far from the preferred binding region were shown to have little or no effect on protein binding behavior [30].

While chromatography experiments can provide an overall indication of protein binding, they are unable to provide detailed insight into the number, location, and relative strength of the ligand interactions with a protein surface. Further, it was of interest to determine how the identified preferred binding region on ubiquitin was affected by this single-site mutation. Would the preferred binding region remain intact or would some or all of it be eliminated? How far from the site of mutation can its effects be perceived? These key questions were examined using NMR chemical shift perturbation mapping and molecular dynamics simulations as described in the subsequent sections.

3.2. NMR chemical shift perturbation mapping

As described in the introduction, NMR was previously employed to identify sites of specific protein–multimodal ligand interactions in solution [30]. Fig. 1 presents a surface representation of ubiquitin colored according to the experimentally determined binding sites. One high affinity site was identified with a dissociation constant of 0.4 mM (±0.1 mM), along with several surrounding binding sites of intermediate affinity. The clustering of binding sites and geometrical considerations led to the proposition that this was a preferred binding region on the protein surface.

2D ^{1}H–^{15}N HSQC spectra were acquired with $^{13}C/^{15}N$-labeled ubiquitin mutant K6E in the absence and presence of NMR buffer containing multimodal ligand (Fig. 2) at the limit of saturation (3.2 mM). In these experiments, resonances of protein amide groups that come into close proximity and interact with the ligand experience a change in chemical shift due to perturbations in the local electronic environment. These perturbations may include desolvation of the ligand–protein interface as well as contributions from small changes in protein side-chain dynamics and packing. As a result, ligand-induced changes in the chemical shifts of the amide

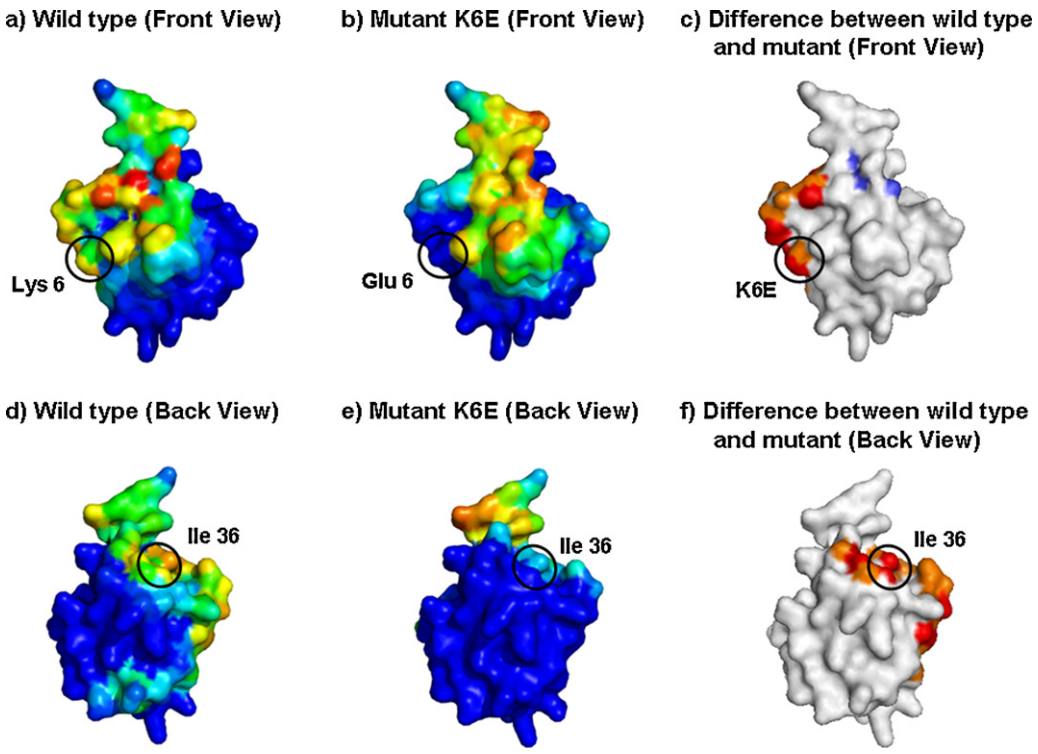

Fig. 5. Molecular dynamics simulation results for wild type ubiquitin and mutant K6E in the presence of a multimodal cation exchange ligand. (a–c) Wild type, mutant K6E, and the difference between the wild type and mutant proteins, respectively (front views); (d–f) Wild type, mutant K6E, and the difference between the wild type and mutant proteins, respectively (back views). Surfaces in (a), (b), (d), and (e) are colored based on the counting method described in the simulation results section, where blue indicates the least interacting sites and red indicates the sites of greatest interaction (blue < cyan < green < yellow < orange < red). The average occupancy of sites over time has been normalized such that red indicates an average occupancy of 39% while blue indicates no occupancy at any time. Surfaces in (c) and (f) are colored based on the difference between the wild type and mutant K6E simulation results where blue indicates greater ligand interaction with the mutant, and orange and red indicate greater interaction with the wild type (blue < white < orange < red). White indicates residues for which the difference between the wild type and mutant is within the margin of error in the simulations. (For interpretation of the references to color in this figure legend, the reader is referred to the web version of the article.)

groups served as reporters of ligand–protein interactions. A single resonance peak for both the unbound and ligand bound form of the protein was observed for each amide group with line widths largely free of exchange broadening and ligand-dependent chemical shift values characteristic of 'fast exchange' behavior between unbound and bound states.

Spectra are presented in Fig. 3 that illustrate ligand-induced chemical shift perturbations for selected residues, including several residues located within the previously identified preferred binding region. Data are presented for both the wild type and mutant protein in the absence and presence of the multimodal ligand. As can be seen in the figure, some residues (e.g., Val 70) exhibited nearly identical chemical shift perturbations for the wild type and mutant proteins. In contrast, some residues exhibited large chemical shift perturbations for the wild type but very small chemical shift perturbations for the mutant. Significant differences were detected for both well-resolved peaks from residues comprising the high affinity binding site (Lys 6 and Ile 44), as well as a neighboring charged residue (His 68).

Ligand-induced changes in amide chemical shift were calculated for each amino acid of the wild type and mutant proteins. Fig. 4a shows the difference in the maximum weighted average change in chemical shift ($\Delta\Delta\delta_{NH}$) between the wild type and mutant proteins. As can be seen in the figure, there are clear differences in the chemical shift perturbations for these two proteins. The data are also illustrated as ribbon (Fig. 4b) and surface (Fig. 4c and d) representations of the protein that are colored according to the magnitude of the change in the weighted average chemical shift perturbations between the wild type and mutant proteins. Residues that exhibited large, intermediate, and small differences in chemical shift perturbation are shown in red, orange, and brown, respectively. Residues exhibiting little or no difference in chemical shift perturbation are shown in blue. The cutoff values used to categorize the chemical shift perturbations are given in the figure legend.

As can be seen in Fig. 4, many of the residues with significant differences in chemical shift perturbation were located within the previously identified preferred binding region (Fig. 1). As expected, residue 6 was identified as having a significant difference in chemical shift perturbation between the wild type and mutant forms. Upon further analysis, it can be seen that several of the surrounding residues also experienced significant changes in chemical shift perturbation due to the mutation at Lys 6. These included Ile 13, Ala 46, and His 68, which exhibited major chemical shift perturbation differences as indicated in red in Fig. 4. Further, Ile 44, Gly 47, Lys 48, and Gln 49 also exhibited noteworthy changes in chemical shift perturbation and are shown in Fig. 4c as a brown cluster on the protein surface residing directly within the preferred binding region.

The fact that several residues in adjoining regions to residue 6 also experienced decreases in chemical shift perturbation due to the mutation is interesting. It suggests that Lys 6 plays a crucial role in the protein–ligand binding interactions not just at the high affinity binding site (residues 6 and 44) but also at some of the surrounding sites. By replacing the lysine residue with glutamic acid, it is likely that the negatively charged ligand was no longer inclined to bind through electrostatic interactions in this region. It is postulated that in a typical multimodal ligand binding event, the ligand is attracted toward the surface by long-ranged electrostatic interactions, with hydrophobic interactions only becoming significant

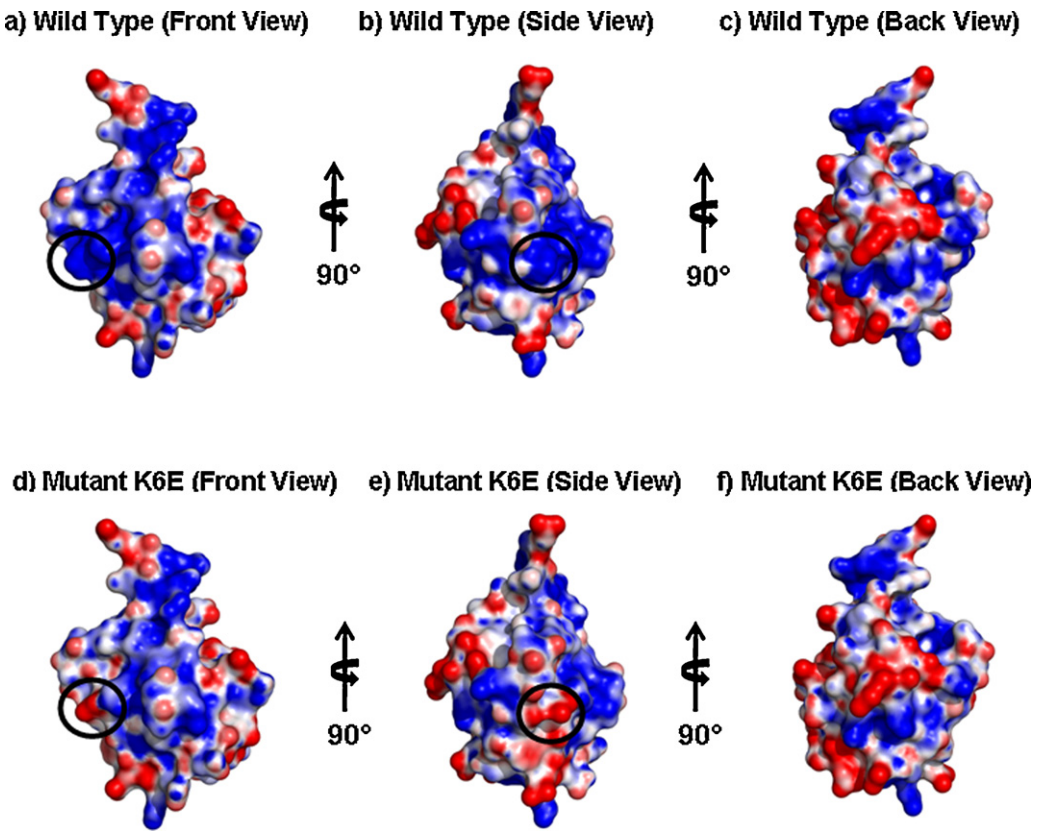

Fig. 6. Electrostatic potential (red = −4 kT/e, blue = +4 kT/e) surface representations for wild type ubiquitin and ubiquitin mutant K6E. (a–c) The front, side, and back views, respectively, for wild type ubiquitin; (d–f) The front, side, and back views, respectively, for mutant K6E. The black circles denote the location of residue 6. (For interpretation of the references to color in this figure legend, the reader is referred to the web version of the article.)

at shorter length scales [32]. By eliminating the favorable electrostatic interactions at position 6, the ligand was less attracted to this region of the protein surface impacting not only the high affinity binding site containing the mutated residue but also several of those in close proximity.

While chemical shift perturbation data can be useful in understanding protein–ligand binding interactions, interpretation of these data can be complicated by a number of factors. Most notably, residues on the periphery of an interaction site which may not be directly interacting with the ligand may undergo a chemical shift perturbation due to their proximity to the interaction site. Further, a residue in direct contact with the ligand may not necessarily undergo a significant change in chemical shift.

3.3. Simulation results

MD simulations were carried out to further examine the effect of mutation on protein–ligand binding behavior at an atomic level. A comparison of the simulations performed with the wild type and mutant protein is shown in Fig. 5. To evaluate the interaction between a ligand and the protein atoms, a counting method was developed where ligand contacts with the protein were subdivided into four points with each point representing a different mode of interaction. The center of mass of the aromatic ring, the amide group, the carboxylic group, and the aliphatic chain of the multimodal ligand were each considered to be a potential interaction point between the protein and the ligand. The entire ligand was considered to be "bound" if the distance between a ligand subunit and the nearest protein heavy atom was less than 5.5 Å for at least three subunits simultaneously. Protein heavy atoms were determined to be interacting with the bound ligand if they were within 4.5 Å of any heavy atom of the ligand. These proximity counts were calculated and averaged over all of the simulations and then mapped onto the protein surface as shown in Fig. 5. The protein surfaces shown in Fig. 5a, b, d, and e are colored on a spectrum from blue to red, with blue and red indicating the interaction sites that are least and most frequently populated, respectively. Fig. 5c and f shows the difference between the wild type and mutant K6E where red and orange denote residues with greater proximity counts for the wild type as compared to the mutant, white denotes residues where the difference between the proteins was within the margin of error, and blue denotes residues with greater proximity counts for the mutant as compared to the wild type. As can be seen in the figure, these maps show a significant decrease in the number of protein–ligand interactions between the wild type and mutant proteins. As expected, the binding interactions at residue 6 were nearly eliminated. Further, as was observed from the NMR results, the region surrounding residue 6 also exhibited some significant changes in ligand binding. Interestingly, changes in binding behavior were also observed on the opposite side of the protein surface of the mutated residue, which did not exhibit measurable binding in the NMR experiments. These changes occurred primarily in a hydrophobic cavity in the top right portion of the protein near residue 36 (Fig. 5d–f).

Since mutant K6E has a charge reversal from the wild type, electrostatic potential maps were calculated to differentiate between the electrostatic properties of the two proteins and to gain further insight into their binding to a multimodal ligand. Fig. 6 shows the electrostatic potentials mapped to the surfaces for the front, side, and back of the wild type (Fig. 6a–c) and the mutant (Fig. 6d–f).

As can be seen in the figure, the changes in electrostatic potential that were observed as a result of the single point mutation were located primarily in a small region around residue 6, the site of mutation. Residue 6 is highlighted by a black circle in the figures. Fig. 6a and b shows that a large, continuous region of positive electrostatic potential existed on the wild type protein surface which included the preferred binding face as well as the adjoining side of the protein. In contrast, for the mutant protein, a patch of negative electrostatic potential disrupts this continuous region of positive electrostatic potential (Fig. 6d and e).

It has been proposed previously that long-ranged electrostatic interactions can drive initial steps of protein complex formation [48,49] followed by translational reorientations to form final specific complexes [50,51]. The results presented here suggest that multimodal ligand binding is governed by a similar mechanism where long-ranged non-specific electrostatic attractions likely constitute the initial steps of the binding process, which steer the ligand closer to the protein surface. Once localized to this particular region, the ligand likely explores multiple potential binding sites where short-ranged interactions including hydrophobic interactions, van der Waals contacts, and hydrogen bonding provide synergistic interactions resulting in high affinity to key residues. In contrast, with the mutant protein, electrostatic repulsion near the site of mutation resulted in weaker binding throughout this extensive interaction surface. Reversing the charge in the mutant breaks the continuous positive patch and repels the MM ligand, thus inhibiting its interaction not only with residue 6 but also with the surrounding region, including some residues on the back side of the protein that lie next to this region (around residue 13) and in the general vicinity of the hydrophobic pocket (near residue 36).

4. Conclusions

The nature of protein adsorption in multimodal chromatographic systems was examined using site-directed mutagenesis, NMR, chromatography, and MD simulations. A ubiquitin mutant was designed to probe a previously identified preferred binding region on the protein surface. The binding of a multimodal ligand, which was likely binding to this area through multipoint attachment prior to mutation, was significantly hindered by a charge reversal at Lys 6. The mutant protein exhibited dramatically weaker chromatographic retention as compared to the wild type protein. Further, the NMR results indicated that the ligand-induced changes in chemical shift decreased substantially at the site of mutation and also for several other residues in the preferred binding region. MD simulations were also used to examine binding interactions in free ligand systems. Although the fundamental differences in the underlying principles of these techniques make quantitative comparisons impractical, it was clear that the MD simulation results were in qualitative agreement with the weaker binding observed with the chromatography and NMR results, and confirmed that residues within the preferred binding region were dramatically affected by the mutation. This was explained by a binding mechanism where electrostatic interactions localize the multimodal ligand to the protein surface and subsequent synergistic interactions of the ligand to key residues provide high binding affinities. The absence of electrostatic attraction at residue 6 resulted in significantly weaker binding of the ligand in this region of the mutant protein.

This work provides an improved understanding of protein binding affinity in multimodal chromatography as well as the effect of mutation on protein–ligand binding interactions. While this work has focused on the protein ubiquitin, the insight gained regarding multimodal ligand binding can be employed in a wide range of systems where protein–ligand interactions play an important role (e.g., bioseparations, biomaterials, drug delivery). Finally, while the NMR and MD studies presented here have focused on ligand–protein binding in solution, it will be important to examine protein binding to solid resin systems containing the multimodal ligand in order to elucidate avidity and steric effects in these systems.

Acknowledgements

This work was partially supported by NSF Grant CBET 0933169. We also thank George Makhatadze, Mayank Patel, and Werner Streicher for their assistance with the expression of the isotopically enriched ubiquitin.

References

[1] M.R. Melander, Z. El Rassi, C. Horvath, J. Chromatogr. 469 (1989) 3.
[2] W.S. Hancock, J.T. Sparrow, J. Chromatogr. 206 (1981) 71.
[3] L.W. McLaughlin, Chem. Rev. 89 (1989) 309.
[4] S.C. Burton, N.W. Haggarty, D.R.K. Harding, Biotechnol. Bioeng. 56 (1997) 45.
[5] S.C. Burton, D.R.K. Harding, J. Chromatogr. A 775 (1997) 39.
[6] B.L. Johansson, M. Belew, S. Eriksson, G. Glad, O. Lind, J.L. Maloisel, N. Norrman, J. Chromatogr. A 1016 (2003) 35.
[7] B.L. Johansson, M. Belew, S. Eriksson, G. Glad, O. Lind, J.L. Maloisel, N. Norrman, J. Chromatogr. A 1016 (2003) 21.
[8] W. Bicker, M. Lammerhofer, W. Lindner, Anal. Bioanal. Chem. 390 (2008) 263.
[9] B.K. Nfor, M. Noverraz, S. Chilamkurthi, P.D.E.M. Verhaert, L.A.M. van der Wielen, M. Ottens, J. Chromatogr. A 1217 (2010) 6829.
[10] K. Kallberg, K. Becker, L. Bülow, J. Chromatgr. A 1218 (2011) 678.
[11] R. Bischoff, L.W. McLaughlin, J. Chromatogr. 270 (1983) 117.
[12] R. Bischoff, L.W. McLaughlin, J. Chromatogr. 296 (1984) 329.
[13] R. Bischoff, L.W. McLaughlin, J. Chromatogr. 317 (1984) 251.
[14] J.T. Eleveld, H.A. Claessens, J.L. Ammerdorffer, A.M. van Herk, C.A. Cramers, J. Chromatogr. A 677 (1994) 211.
[15] J. Chen, J. Tetrault, Y. Zhang, A. Wasserman, G. Conley, M. DiLeo, E. Haimes, A.E. Nixon, A. Ley, J. Chromatogr. A 1217 (2010) 216.
[16] K.A. Kaleas, C.H. Schmelzer, S.A. Pizarro, J. Chromatogr. A 1217 (2010) 235.
[17] J. Clarkson, I.D. Campbell, Biochem. Soc. Trans. 31 (2003) 1006.
[18] J. Song, J.L. Markley, J. Mol. Recognit. 14 (2001) 166.
[19] D.W. Byerly, C.A. McElroy, M.P. Foster, Protein Sci. 11 (2002) 1850.
[20] G.W. Daughdrill, G.W. Buchko, M.V. Botuyan, C. Arrowsmith, M.S. Wold, M.A. Kennedy, D.F. Lowry, Nucleic Acids Res. 31 (2003) 4176.
[21] H.Y. Hu, J.K. Korton, M.R. Gryk, R. Prasad, J.M. Naron, D.A. Sun, S.M. Hecht, S.H. Wilson, G.P. Mullen, J. Biol. Chem. 279 (2004) 39736.
[22] X. Xu, S.K. Kim, P. Schürmann, M. Hirasawa, J.N. Tripathy, J. Smith, D.B. Knaff, M. Ubbink, FEBS Lett. 580 (2006) 6714.
[23] A. Medek, P.J. Hajduk, J. Mack, S.W. Fesik, J. Am. Chem. Soc. 122 (2000) 1241.
[24] Y.H. Hong, H.C. Ahn, J. Lim, H.M. Kim, H.Y. Ji, S. Lee, J.H. Kim, E.Y. Park, H.K. Song, B.J. Lee, FEBS Lett. 583 (2009) 287.
[25] R.C. Lu, X.R. Guo, C. Jin, J.X. Xiao, Biochim. Biophys. Acta 1790 (2009) 134.
[26] M.J. Kelly, L.J. Ball, C. Krieger, Y. Yu, M. Fischer, S. Schiffmann, P. Schmieder, R. Kuhne, W. Bermel, A. Bacher, G. Richter, H. Oschkinat, Proc. Natl. Acad. Sci. U.S.A. 98 (2001) 13025.
[27] C. Groger, A. Moglich, M. Pons, B. Koch, W. Hengstenberg, H.R. Kalbitzer, E. Brunner, J. Am. Chem. Sci. 125 (2003) 8726.
[28] A. Ciulli, G. Williams, A.G. Smith, T.L. Blundell, C. Abell, J. Med. Chem. 49 (2006) 4992.
[29] W.K. Chung, Y. Hou, M. Holstein, A. Freed, G.I. Makhatadze, S.M. Cramer, J. Chromatogr. A 1217 (2010) 191.
[30] W.K. Chung, A.S. Freed, M.A. Holstein, S.A. McCallum, S.M. Cramer, Proc. Natl. Acad. Sci. U.S.A. 107 (2010) 16811.
[31] A. Bhinge, P. Chakrabarti, K. Uthanumallian, K. Bajaj, K. Chakraborty, R. Varadarajan, Structure 12 (2004) 1989.
[32] A.S. Freed, S. Garde, S.M. Cramer, J. Phys. Chem. B 115 (2011) 13320.
[33] P.L. Wintrode, G.I. Makhatadze, P.L. Privalov, Proteins 18 (1994) 246.
[34] T.D. Goddard, D.G. Kneller, SPARKY 3, University of California, San Francisco.
[35] G.S. Rule, T.K. Hitchens, Fundamentals of Protein NMR Spectroscopy, Springer, New York, 2005.
[36] B.T. Farmer, K.L. Constantine, V. Goldfarb, M.S. Friedrichs, M. Wittekind, J. Yanchunas, J.G. Robertson, L. Mueller, Nat. Struct. Biol. 3 (1996) 995.
[37] The PyMOL Molecular Graphics System, Version 1.1, Schrodinger, LLC.
[38] W.D. Cornell, P. Cieplak, C.I. Bayly, I.R. Gould, K.M. Merz, D.M. Ferguson, D.C. Spellmeyer, T. Fox, J.W. Caldwell, P.A. Kollman, J. Am. Chem. Soc. 117 (1995) 5179.
[39] Molecular Operating Environment, Chemical Computing Group, Inc., Montreal, Quebec, Canada, 2010.
[40] H.J.C. Berendsen, J.R. Grigera, T.P. Straatsma, J. Phys. Chem. 91 (1987) 6269.
[41] E. Lindahl, B. Hess, D. van der Spoel, J. Mol. Model. 7 (2001) 306.
[42] H.J.C. Berendsen, D. van der Spoel, R. Van Drunen, Comput. Phys. Commun. 91 (1995) 43.

[43] S. Nose, J. Chem. Phys. 81 (1984) 511.
[44] D.J. Evans, B.L. Holian, J. Chem. Phys. 83 (1985) 4069.
[45] M. Parrinello, A. Rahman, Phys. Rev. Lett. 45 (1980) 1196.
[46] P.P. Ewald, Ann. Phys. 64 (1921) 253.
[47] W. Humphrey, A. Dalke, K. Schulten, J. Mol. Graph. 14 (1996) 33.
[48] O.G. Berg, P.H. von Hippel, Ann. Rev. Biophys. Biophys. Chem. 14 (1985) 131.
[49] M.E. Davis, J.D. Madura, J. Sines, B.A. Luty, S.A. Allison, J.A. McCammon, Methods Enzymol. 202 (1991) 473.
[50] C. Tang, J. Iwahara, G.M. Clore, Nature 444 (2006) 383.
[51] J.Y. Suh, C. Tang, G.M. Clore, J. Am. Chem. Soc. 129 (2007) 12954.